LETTER

Synchronized cycles of bacterial lysis for *in vivo* delivery

M. Omar Din[1]*, Tal Danino[2]†*, Arthur Prindle[1], Matt Skalak[2], Jangir Selimkhanov[1], Kaitlin Allen[2], Ellixis Julio[1], Eta Atolia[2], Lev S. Tsimring[3], Sangeeta N. Bhatia[2,4,5,6,7,8]§ & Jeff Hasty[1,3,9]§

The widespread view of bacteria as strictly pathogenic has given way to an appreciation of the prevalence of some beneficial microbes within the human body[1–3]. It is perhaps inevitable that some bacteria would evolve to preferentially grow in environments that harbour disease and thus provide a natural platform for the development of engineered therapies[4–6]. Such therapies could benefit from bacteria that are programmed to limit bacterial growth while continually producing and releasing cytotoxic agents *in situ*[7–10]. Here we engineer a clinically relevant bacterium to lyse synchronously at a threshold population density and to release genetically encoded cargo. Following quorum lysis, a small number of surviving bacteria reseed the growing population, thus leading to pulsatile delivery cycles. We used microfluidic devices to characterize the engineered lysis strain and we demonstrate its potential as a drug delivery platform via co-culture with human cancer cells *in vitro*. As a proof of principle, we tracked the bacterial population dynamics in ectopic syngeneic colorectal tumours in mice via a luminescent reporter. The lysis strain exhibits pulsatile population dynamics *in vivo*, with mean bacterial luminescence that remained two orders of magnitude lower than an unmodified strain. Finally, guided by previous findings that certain bacteria can enhance the efficacy of standard therapies[11], we orally administered the lysis strain alone or in combination with a clinical chemotherapeutic to a syngeneic mouse transplantation model of hepatic colorectal metastases. We found that the combination of both circuit-engineered bacteria and chemotherapy leads to a notable reduction of tumour activity along with a marked survival benefit over either therapy alone. Our approach establishes a methodology for leveraging the tools of synthetic biology to exploit the natural propensity for certain bacteria to colonize disease sites.

In order to control population levels and facilitate drug delivery using bacteria, we engineered a synchronized lysis circuit (SLC) using coupled positive and negative feedback loops that have previously been used to generate robust oscillatory dynamics[12,13]. The circuit (Fig. 1a) consists of a common promoter that drives expression of both its own activator (positive feedback) and a lysis gene (negative feedback). Specifically, the *luxI* promoter regulates production of autoinducer (AHL), which binds LuxR and enables it to transcriptionally activate the promoter. Negative feedback arises from cell death that is triggered by a bacteriophage lysis gene (φX174 E) which is also under control of the *luxI* promoter[13–15]. AHL can diffuse to neighbouring cells and thus provides an intercellular synchronization mechanism.

The bacterial population dynamics arising from the synchronized lysis circuit can be conceptualized as a slow build-up of the signalling molecule (AHL) to a threshold level, followed by a lysis event that rapidly prunes the population and enables the release of bacterial contents (Fig. 1b). After lysis, a small number of remaining bacteria begin to produce AHL anew, allowing the 'integrate and fire' process to be repeated in a cyclical fashion. We used microfluidic devices to observe growth and lysis with the fluorescent protein superfolder GFP (sfGFP) as a proxy for circuit dynamics in attenuated *Salmonella enterica* subsp. *enterica* serovar Typhimurium (Supplementary Videos 1 and 2). We observed periodic lysis events characterized by peaks in the fluorescent reporter expression that correspond to population lysis (Fig. 1c). The fraction of lysed cells remains consistent across subsequent cycles, suggesting that lysis and survival occur in a stochastic manner (Extended
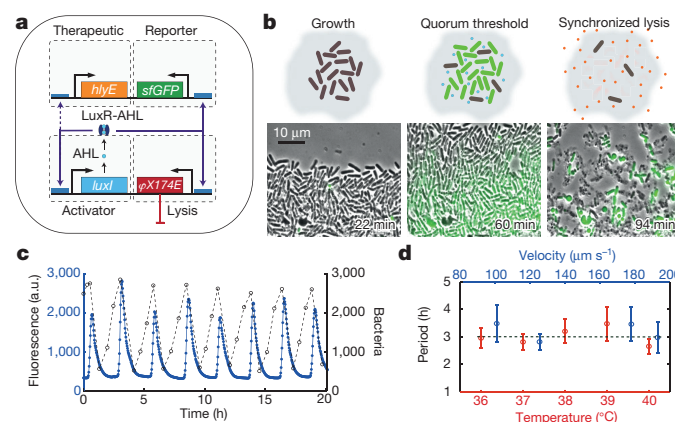

Figure 1 | Construction and characterization of the SLC. a, The circuit contains an activator[13] and lysis plasmid. When the population reaches the quorum threshold at a critical AHL concentration, the *luxI* promoter drives the transcription of gene *E* for lysis, *luxI*, and *sfGFP* or *luxCDABE* as the reporter module. The *luxI* or the *tac* promoter also drives the transcription of the therapeutic gene for the stabilized circuit used *in vivo*. LuxR in this system is driven by the native *luxR* promoter. **b**, The main stages of each lysis cycle from seeding to quorum 'firing'. Shown below the schematic depictions are typical time series images of the circuit-harbouring cells undergoing the three main stages of quorum firing in a microfluidic growth chamber[12]. **c**, Fluorescence profile of a typical microfludic experiment. The estimated cell population trajectory reveals that lysis events correspond to peaks of sfGFP fluorescence. **d**, Period as a function of estimated flow velocity in the media channel of the microfluidic device and environmental temperature. Error bars indicate ± 1 s.d. for 13–50 peaks. These experiments were performed with strain 1, see Supplementary Information for complete strain information.

[1]Department of Bioengineering, University of California, San Diego, La Jolla, California 92093, USA. [2]Institute for Medical Engineering & Science, Massachusetts Institute of Technology, Cambridge, Massachusetts 02139, USA. [3]BioCircuits Institute, University of California, San Diego, La Jolla, California 92093, USA. [4]Broad Institute of Harvard and MIT, Cambridge, Massachusetts 02139, USA. [5]Department of Medicine, Brigham and Women's Hospital, Boston, Massachusetts 02139, USA. [6]Electrical Engineering and Computer Science and David H. Koch Institute for Integrative Cancer Research, Massachusetts Institute of Technology, Cambridge, Massachusetts 02139, USA. [7]Marble Center for Cancer Nanomedicine and Ludwig Center for Molecular Oncology, Massachusetts Institute of Technology, Cambridge, Massachusetts 02139, USA. [8]Howard Hughes Medical Institute, Chevy Chase, Maryland 20815, USA. [9]Molecular Biology Section, Division of Biological Science, University of California, San Diego, La Jolla, California 92093, USA. †Present address: Department of Biomedical Engineering, Columbia University, New York, New York 10027, USA.
*These authors contributed equally to this work.
§These authors jointly supervised this work.
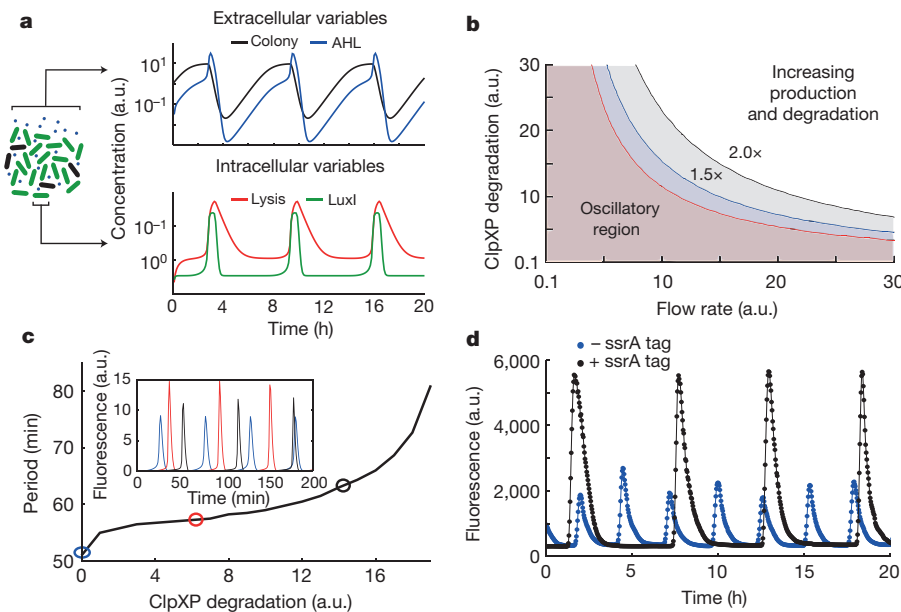
Figure 2 | Computational modelling and tunability. a, The model consists of intracellular variables (lysis protein E and LuxI concentrations) and extracellular variables (colony size and AHL concentrations). A time series of colony size (black), colony AHL (blue), intracellular LuxI (green) and lysis protein concentrations (red) are shown on the right. **b**, The region in the model parameter space for ClpXP-mediated degradation (see Supplementary Information) and flow where the model output is oscillatory increases with higher production and degradation terms. **c**, Results from the computational model showing the ability to tune the oscillatory period by varying ClpXP mediated degradation of LuxI. **d**, Fluorescence profiles showing lysis oscillations for LuxI ssrA (black, strain 2) and LuxI non-ssrA (blue, strain 1) tagged versions of the circuit. See Supplementary Information for complete model information.

Data Fig. 1a, b). Given the ultimate goal of implementation in an *in vivo* microenvironment characterized by variable growth conditions, we tested a range of incubation temperatures (36 °C to 40 °C) and perfusion rates (100 μm s⁻¹ to 200 μm s⁻¹), measuring an average period of 3 h across all conditions (Fig. 1d). These findings demonstrate that the SLC has the capacity to generate robust cycles of bacterial lysis in our microfluidic devices across a spectrum of environmental fluctuations that is likely to exist in an *in vivo* context.

The emergence of bacterial therapies in synthetic biology has accentuated the need for predictive modelling. This need stems from a bottleneck created by a difference in the timescales for bacterial cloning versus animal experiments; the circuits required for candidate therapies can be created much faster than they can be tested *in vivo*. Therefore, in order to quantitatively characterize the SLC concept before testing in a lower-throughput animal model setting, we developed a computational model (Fig. 2a and Supplementary Information) to define an optimal strategy for subsequent testing in a lower-throughput animal model setting. We found that high production and degradation rates of the feedback-controlling proteins resulted in a wider domain of oscillatory dynamics in the parameter space (Fig. 2b). This model is consistent with our observations that oscillations in *S.* Typhimurium were more robust than in *Escherichia coli*, in which rates of protein production and degradation were previously found to be lower[16] (Extended Data Fig. 1c and Supplementary Video 3). As the ability to manipulate circuit behaviour enhances the versatility of the system, we explored the tunability of the lysis period by adding an ssrA degradation tagging sequence on the LuxI protein. Consistent with model predictions, we observed an increased period and colony firing amplitude when tracking bacterial population dynamics (Fig. 2c, d and Extended Data Fig. 1d). The SLC thus enables tuning of the period and magnitude of delivery, which will be necessary for eventual application of this platform in the complex and fluctuating conditions present *in vivo*.

To incorporate a cytotoxic payload into the SLC strain, we added expression of Haemolysin E, encoded by *hlyE* of *E. coli*, which has been tested as a pore-forming anti-tumour toxin[17]. We initially confirmed the capability of the circuit to release intracellular contents by visualizing released sfGFP with a small microfluidic sink located beneath the growth chamber (Extended Data Fig. 2a–c). Then to visualize bacterial lysis and killing of cancer cells *in vitro* via HlyE, we engineered a microfluidic device so that cancer cells adhere inside a growth channel that is flanked by smaller bacterial growth chambers, which permits simultaneous single-cell visualization of bacterial lysis and cancer cell death (Extended Data Fig. 2d). After co-culturing human cervical cancer HeLa cells with *S.* Typhimurium harbouring the SLC circuit, we observed HeLa cell death upon the onset of bacterial lysis, indicating efficient toxin release (Fig. 3a, b and Supplementary Videos 4 and 5). Complete cell death occurred in the growth channel within ~111 min of initial sfGFP fluorescence (Fig. 3c). Thus, the SLC bacteria were capable of releasing HlyE at levels necessary to kill tumour-derived cells.

We assessed the toxicity of released SLC or control bacterial contents in batch culture. As anticipated, we found that HeLa cells exposed to supernatant from a culture of the SLC bacteria bearing the *hlyE* module exhibited almost complete loss of viability (Fig. 3d), whereas the viability of HeLa cells exposed to supernatants of bacteria bearing the *hlyE* module without the SLC and equivalent dose of non-payload bearing SLC bacteria were only slightly affected (~15%). We concluded that bacterial lysis allowed for efficient HlyE release *in vitro* and that natural intracellular bacterial contents do not significantly affect HeLa cell viability. We further investigated the delivery characteristics of the SLC bacteria with *hlyE* by seeding variable amounts of circuit-harbouring bacteria with HeLa cultures in well plates. We observed that the time to HeLa cell death following initial seeding increased with lower bacterial seeding volumes, presumably resulting from the extended time needed for bacteria to reach the quorum threshold (Fig. 3e and Supplementary Video 6). Initial seeding with a larger volume of bacteria resulted in increased firing rates which corresponded to shorter HlyE exposure times until cell death, consistent with a greater magnitude of lysis and payload release, although the cumulative toxicity threshold appears to be similar in all cases (Fig. 3f). On the basis of these observations, the seeding size of the bacterial population can be adjusted to determine the initial timing and release characteristics of the circuit.

We used a luciferase reporter to monitor bacterial population dynamics in grafted syngeneic colorectal tumours in mice. To minimize the extent of plasmid loss in the absence of antibiotic selection *in vivo*, we incorporated previously described stabilizing elements for plasmid retention and segregation into the SLC strain[18–22]. Additionally, we placed both the payload and *luxCDABE* genes (the *in vivo* reporter module) under the *luxI* promoter as an indicator of *hlyE* production and quorum firing via bacterial luminescence (Fig. 1a). Using a subcutaneous model of colorectal cancer (MC26 cell line) in immunocompetent mice, we intratumorally injected a strain of SLC bacteria (SLC-hly). We observed pulsatile bacterial population dynamics within the tumour (Fig. 4a–c and Extended Data Fig. 3a, b) using *in vivo* imaging technology[23], consistent with the design and *in vitro* characterization (Fig. 2). The end luminescence intensity was on
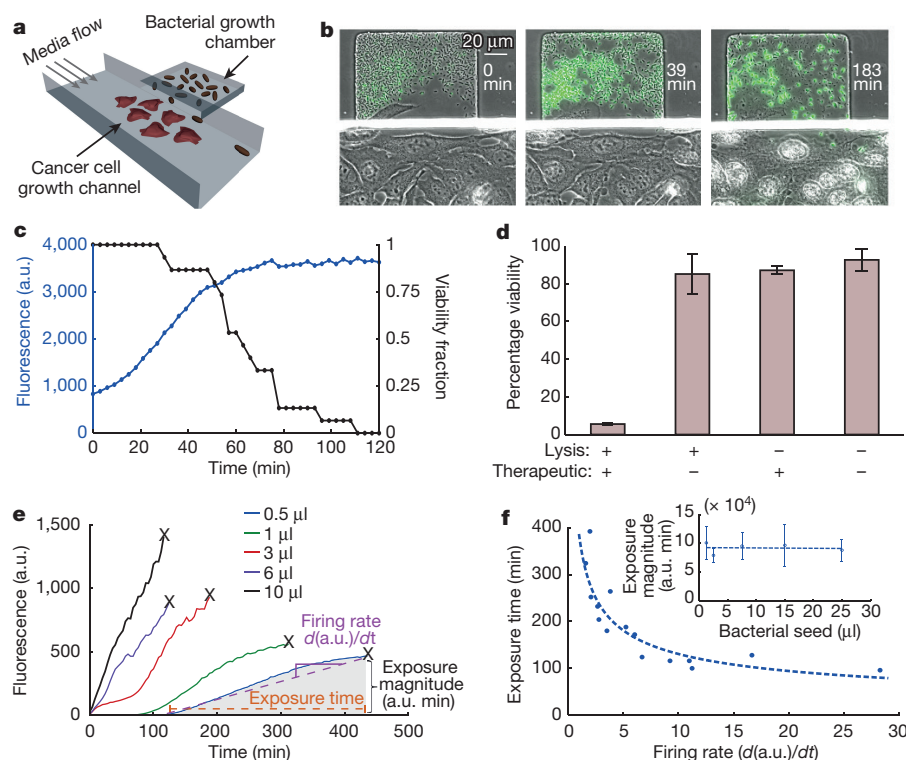
Figure 3 | *In vitro* co-culture. a, Schematic of the microfluidic co-culture with cancer cells and bacteria. Fluidic resistance was modified in this chip to achieve stable near-stagnant flow reduction to allow for cancer cell adherence and for diffusion of released therapeutic from the trap to the channel (see Supplementary Information). **b**, Frames from the co-culture time series sequentially visualizing *S*. Typhimurium (strain 3) firing, lysis and HeLa cell death. **c**, Fluorescent profile of the bacteria and HeLa cell viability fraction (number of live cells / number of dead cells in image frames) from **b** with time. **d**, Percentage viability of HeLa cells co-cultured with supernatant from *S*. Typhimurium culture harbouring the SLC + HlyE (strain 4), the SLC only (strain 5), constitutive *hlyE* only (strain 6), or no plasmid (strain 7). Error bars indicate ± 1 s.e. averaged over three measurements. **e**, Fluorescence profile of the SLC + HlyE (strain 4) co-cultured with HeLa cells at various initial seeding densities. The x symbols on the graph mark the point of complete HeLa cell death. **f**, The toxin exposure time, measured from the initial presence of fluorescence to HeLa cell death, as a function of the sfGFP production rate (see example in **e**). Although the time to death depends on seeding, the total magnitude of exposure remains conserved (inset). Error bars indicate ± 1 s.e. for three measurements. See Supplementary Information for ELH1301 host strain information.
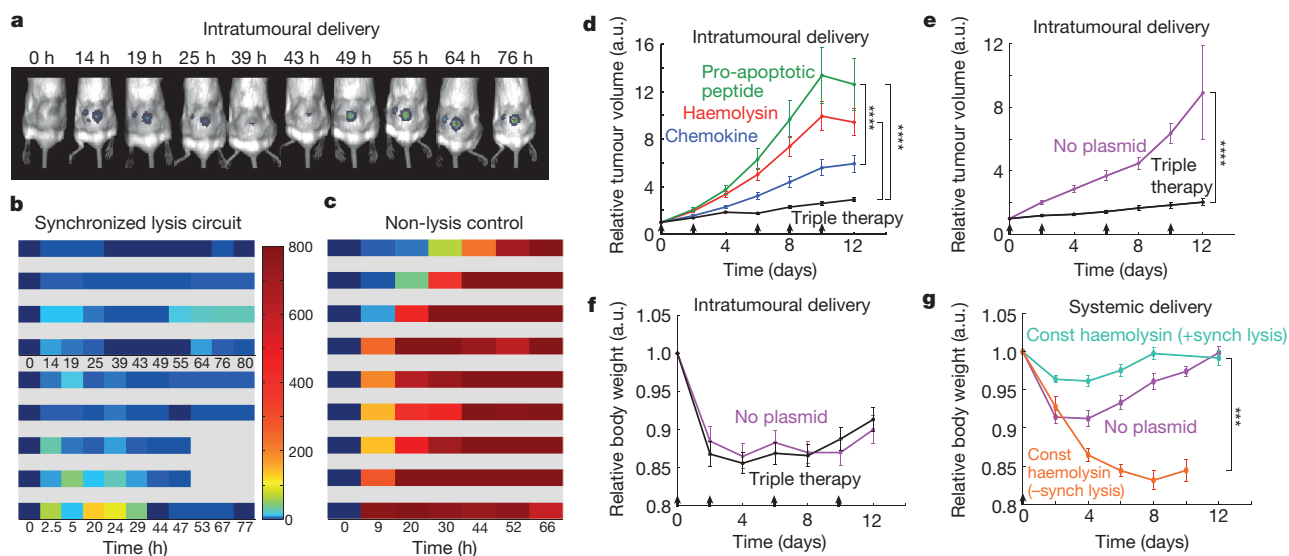
Figure 4 | *In vivo* bacterial dynamics, effect on tumours and tolerability in a subcutaneous tumour model. a, *In vivo* imaging over time of a mouse bearing two hind flank tumours injected once with the stabilized SLC-hly strain (strain 8). **b**, Single tumour density map trajectories of bacterial luminescence (relative to luminescence at 0 h) for the SLC-hly strain (strain 8). Data for each axis represents separate experiments. **c**, Single tumour density map trajectories of bacterial luminescence for the genomically integrated constitutively luminescent strain (strain 9). Intratumoral injection resulted in over 35-fold higher post-injection luminescence compared to intravenous injection (Extended Data Fig. 3d). **d**, Average relative tumour volume over time for subcutaneous tumour bearing mice injected with SLC-hly (red, strain 10), SLC-cdd (green, strain 14), SLC-ccl21 (blue, strain 15), and all together (SLC-3) (black). Bacteria were injected intratumorally on days 0, 2, 6, 8, and 10 (black arrows) (****$P < 0.0001$, two-way ANOVA with Bonferroni post-test, $n = 14$–17 tumours, error bars show s.e.). **e**, Average relative tumour volume over

time for mice with subcutaneous tumours injected with the SLC-3 strains (black, strains 10, 14 and 15) and the no-plasmid control (magenta, strain 7). Bacteria were injected intratumorally on days 0, 2, 6, and 10 (black arrows) (****$P < 0.0001$, two-way ANOVA with Bonferroni post-test, $n = 18$–19 tumours, error bars represent s.e.). **f**, Average relative body weight over time for mice with subcutaneous tumours injected with the SLC-3 strains (black, strain 10, 14, and 15) and the no-plasmid control (magenta, strain 7). Bacteria were injected intratumorally on days 0, 2, 6, and 10 (black arrows) ($n = 10$ mice for both cases, error bars represent s.e.). **g**, Average relative body weight over time for subcutaneous tumour-bearing mice with a single intravenous injection of the SLC + constitutive hlyE (turquoise, $n = 9$ mice, strain 11), a non-SLC strain with constitutive hlyE (orange, $n = 5$ mice, strain 12), or the no-plasmid control strain (magenta, $n = 9$ mice, strain 7) (***$P < 0.001$, two-way ANOVA with Bonferroni post-test, error bars represent s.e.).
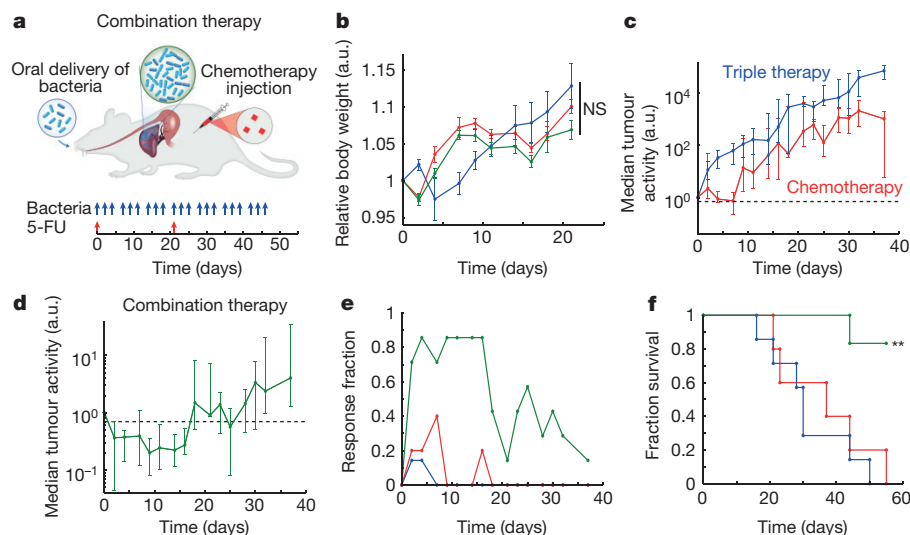
Figure 5 | *In vivo* testing in an experimental model of colorectal metastases in the liver via oral delivery of bacteria. a, Schematic of the experimental syngeneic transplantation model of hepatic colorectal metastases in a mouse, with the dosing schedule of either engineered bacteria (SLC-3) or a common cytotoxic chemotherapeutic, the antimetabolite 5-FU. The SLC-3 strains were delivered orally. 5-FU was delivered via intraperitoneal injection. **b**, Relative body weight over time for the mice with hepatic colorectal metastases fed with the SLC-3 strains (blue), injected with 5-FU chemotherapy (red), or a combination of the two (green). Error bars indicate ± 1 s.e. for 5–7 mice. **c**, Median relative tumour activity, measured via tumour cell luminescence using *in vivo* imaging, for the chemotherapy and SLC-3 cases from **b**. **d**, Median relative tumour activity for the combination therapy case from **b**. Error bars for **c** and **d** indicate the interquartile ranges for 5–7 mice. The dashed line marks relative tumour activity of 0.70. **e**, Fraction of mice from the cases in **b** which respond with 30% reduction of tumour activity over time. **f**, Fraction survival over time for the mice in **b** (**P < 0.01, log rank test; n = 5–7 mice).

average ∼300-fold lower than the constitutive control strain, indicating a significant decrease in bacterial population levels within the tumour (Extended Data Fig. 3c).

Given the ability to engineer bacterial population dynamics in tumour grafts, we leveraged the versatility of the SLC bacteria as a delivery system to compare different classes of previously developed payloads. In addition to the haemolysin strain that was characterized in microfluidic devices, we created two additional SLC strains expressing genes to activate a host immune response (via T-cell and dendritic cell recruitment, using mouse CCL21) or trigger tumour cell apoptosis (using the cell death domain of Bit1 fused to the tumour-penetrating peptide iRGD, or CDD-iRGD)[24,25]. Upon intratumoral injection, the immune recruitment strain elicited the strongest effect on tumour growth when compared to the haemolysis or apoptotic strains (Fig. 4d). We observed that an equal mixture of the three strains generated a stronger response than any single strain (Fig. 4d and Extended Data Fig. 3e–g), and on this basis we elected to pursue the 'triple-strain' dose for further testing in order to minimize animal usage. In a side-by-side comparison, we observed that the tumour response to SLC triple-strain (SLC-3) injections was significantly larger than the response to unmodified bacteria (Fig. 4e). Upon necropsy, histopathological analysis of remnant tumours was performed for mice treated with the SLC-3 strains, chemotherapy or unmodified bacteria. In mice treated with SLC-3 and non-circuit bacterial strains, robust staining of bacteria was observed by anti-*Salmonella* antibodies, showing localization of *Salmonella* within tumours. TUNEL staining indicated higher levels of apoptosis and cell death in SLC-3 treated tumours (Extended Data Fig. 4).

As a first step towards monitoring the effect of bacterial injections on the host, we compared how the triple-strain system affected body weight when administered intratumorally and intravenously, as the administration route affects bacterial localization (Extended Data Fig. 3d). We found that treatment with the SLC strains generated the same weight change as unmodified bacteria when administered intratumorally (Fig. 4f). However, intravenous administration of the SLC conferred a greater health benefit on the basis of observations that SLC strains producing constitutive therapy were better tolerated

than unmodified bacteria or non-SLC strains producing constitutive therapy (Fig. 4g). Although further targeted studies are required to systematically explore the effect of these bacteria on host health, these preliminary experiments suggest that the SLC design can reduce the burden of bacterial injections.

To explore a proof-of-principle for the application of our circuit in the context of *in vivo* tumours, we examined the efficacy of our system in an experimental syngeneic transplantation model of colorectal metastases within the liver. We had previously established that oral delivery of these bacterial strains led to safe and efficient colonization of hepatic colorectal metastases (see Methods), and that mice tolerated repeated dosing without overt adverse effects (Fig. 5a, b)[22]. In the context of bacteria-based therapeutic candidates, previous studies have shown that anaerobic bacteria can occupy avascular tumour compartments where chemotherapy is thought to be ineffective due to poor drug delivery[11]. Thus a synergistic effect may arise when bacteria are used to deliver drugs to the necrotic core of a tumour, while standard chemotherapy is used for the vascularized regions[11,26]. Inspired by this paradigm, we tested the combination of SLC-3 bacteria with a common clinical chemotherapy of 5-fluorouracil (5-FU). Tumours exhibited similar growth trajectories in response to repeated oral delivery of either the bacterial therapy alone, or two i.v. doses of 5-FU on day 0 and day 21 (Fig. 5c). In contrast, combination of these two applications led to a marked decrease in tumour activity over a period of 18 days, followed by a return to growth (Fig. 5d). During the initial 18-day period, a large fraction of the tumours was scored as eliciting at least a 30% reduction in tumour activity (Fig. 5e). The overall response led to roughly a 50% increase in the mean survival time for animals harbouring incurable colorectal metastases (Fig. 5f). Improvements may arise from strategies for long-term circuit stability or the utilization of additional therapeutic cargo.

The synchronized lysis circuit exemplifies a methodology for leveraging the tools of synthetic biology to exploit the ability of certain bacteria to colonize disease sites. In contrast to most drug delivery strategies, the synchronized lysis paradigm does not require pre-loading of a drug or the engineering of additional secretion machinery. In addition, it has the potential to decrease the likelihood of a systemic

inflammatory response through population control; as the bacterial colony is pruned after each oscillatory lysis event, the design could mitigate an undesirable host response. The circuit may enable new bacterial drug delivery strategies through modulation of the frequency and amplitude of the population cycles over time. Given recent insights into how host metabolism and circadian function are affected by the population dynamics of the gut micobiota, cyclical population control may be a prospective strategy to prevent host disturbances resulting from aberrant oscillations of gut microbes[27,28]. Such engineering strategies may allow for the development of therapeutic communities within *in vivo* environments in which population dynamics are driven by interacting viruses, bacteria and host immune cells[29].

1. Cho, I. & Blaser, M. J. The human microbiome: at the interface of health and disease. *Nature Rev. Genet.* **13**, 260–270 (2012).
2. Xuan, C. *et al.* Microbial dysbiosis is associated with human breast cancer. *PLoS One* **9**, e83744 (2014).
3. Fischbach, M. A., Bluestone, J. A. & Lim, W. A. Cell-based therapeutics: the next pillar of medicine. *Sci. Transl. Med.* **5**, 179ps7 (2013).
4. Pawelek, J. M., Low, K. B. & Bermudes, D. Tumor-targeted *Salmonella* as a novel anticancer vector. *Cancer Res.* **57**, 4537–4544 (1997).
5. Ruder, W. C., Lu, T. & Collins, J. J. Synthetic biology moving into the clinic. *Science* **333**, 1248–1252 (2011).
6. Weber, W. & Fussenegger, M. Emerging biomedical applications of synthetic biology. *Nature Rev. Genet.* **13**, 21–35 (2011).
7. Baban, C. K., Cronin, M., O'Hanlon, D., O'Sullivan, G. C. & Tangney, M. Bacteria as vectors for gene therapy of cancer. *Bioeng. Bugs* **1**, 385–394 (2010).
8. Hoption Cann, S. A., van Netten, J. P. & van Netten, C. Dr William Coley and tumour regression: a place in history or in the future. *Postgrad. Med. J.* **79**, 672–680 (2003).
9. Davila, M. L. *et al.* Efficacy and toxicity management of 19–28z CAR T cell therapy in B cell acute lymphoblastic leukemia. *Sci Transl. Med.* **6**, 224ra25 (2014).
10. Garrett, W. S. Cancer and the microbiota. *Science* **348**, 80–86 (2015).
11. Dang, L. H., Bettegowda, C., Huso, D. L., Kinzler, K. W. & Vogelstein, B. Combination bacteriolytic therapy for the treatment of experimental tumors. *Proc. Natl Acad. Sci. USA* **98**, 15155–15160 (2001).
12. Danino, T., Mondragón-Palomino, O., Tsimring, L. & Hasty, J. A synchronized quorum of genetic clocks. *Nature* **463**, 326–330 (2010).
13. Prindle, A. *et al.* A sensing array of radically coupled genetic 'biopixels'. *Nature* **481**, 39–44 (2011).
14. Young, K. D. & Young, R. Lytic action of cloned φ X174 gene E. *J. Virol.* **44**, 993–1002 (1982).
15. Marguet, P., Tanouchi, Y., Spitz, E., Smith, C. & You, L. Oscillations by minimal bacterial suicide circuits reveal hidden facets of host-circuit physiology. *PLoS One* **5**, e11909 (2010).
16. Prindle, A. *et al.* Genetic circuits in *Salmonella typhimurium*. *ACS Synth. Biol.* **1**, 458–464 (2012).
17. Ryan, R. M. *et al.* Bacterial delivery of a novel cytolysin to hypoxic areas of solid tumors. *Gene Ther.* **16**, 329–339 (2009).
18. Gerdes, K. The *parB* (*hok/sok*) locus of plasmid R1: a general purpose plasmid stabilization system. *Nature Biotechnol.* **6**, 1402–1405 (1988).
19. Wood, T., Kuhn, R. & Peretti, S. Enhanced plasmid stability through post-segregational killing of plasmid-free cells. *Biotechnol. Tech.* **4**, 39–44 (1990).
20. Derman, A. I. *et al.* Phylogenetic analysis identifies many uncharacterized actin-like proteins (Alps) in bacteria: regulated polymerization, dynamic instability and treadmilling in Alp7A. *Mol. Microbiol.* **73**, 534–552 (2009).
21. Danino, T., Lo, J., Prindle, A., Hasty, J. & Bhatia, S. N. *In vivo* gene expression dynamics of tumor-targeted bacteria. *ACS Synth. Biol.* **1**, 465–470 (2012).
22. Danino, T. *et al.* Programmable probiotics for detection of cancer in urine. *Science Transl. Med.* **7**, 289ra84 (2015).
23. Danino, T., Prindle, A., Hasty, J. & Bhatia, S. Measuring growth and gene expression dynamics of tumor-targeted *S. Typhimurium* bacteria. *JoVE* e50540 (2013).
24. Chen, R. *et al.* Application of a proapoptotic peptide to intratumorally spreading cancer therapy. *Cancer Res.* **73**, 1352–1361 (2013).
25. Loeffler, M., Le'Negrate, G., Krajewska, M. & Reed, J. C. *Salmonella typhimurium* engineered to produce CCL21 inhibit tumor growth. *Cancer Immunol. Immunother.* **58**, 769–775 (2009).
26. Forbes, N. S. Engineering the perfect (bacterial) cancer therapy. *Nature Rev. Cancer* **10**, 785–794 (2010).
27. Leone, V. *et al.* Effects of diurnal variation of gut microbes and high-fat feeding on host circadian clock function and metabolism. *Cell Host Microbe* **17**, 681–689 (2015).
28. Thaiss, C. A., Levy, M. & Elinav, E. Chronobiomics: the biological clock as a new principle in host–microbial interactions. *PLoS Pathog.* **11**, e1005113 (2015).
29. Cheong, I. *et al.* A bacterial protein enhances the release and efficacy of liposomal cancer drugs. *Science* **314**, 1308–1311 (2006).

Author Contributions M.O.D. and J.H. designed the synchronized lysis circuit. M.O.D., J.S., L.S.T. and J.H. developed the computational model. M.O.D. and A.P. built and tested the bacterial circuit in microfluidics and performed the co-culture experiments. M.O.D. and E.J. collected the viability data, and M.O.D. and J.H. analysed the bacterial circuit data. T.D., M.S., K.A., and E.A. designed and performed the *in vivo* experiments. M.O.D., T.D., A.P., S.N.B., and J.H. analysed the animal data, and wrote and edited the manuscript.

METHODS

Strains and plasmids. Our circuit strains were cultured in LB media with $50\,\mu g\,ml^{-1}$ and $34\,\mu g\,ml^{-1}$ of kanamycin and chloramphenicol respectively, along with 0.2% glucose, in a 37 °C incubator. Mammalian cells (HeLa CCL-2 from ATCC, verified by third-party cell line authentication services using an STR multiplex system) were cultured in DMEM media supplemented with 10% fetal bovine serum and 1% penicillin/streptomycin (CellGro 30-002-CI), placed inside a tissue culture incubator at 37 °C maintained at 5% CO_2. Plasmids were constructed using the CPEC method of cloning or using standard restriction digest/ligation cloning. The activator plasmid (Kan, ColE1) was used in previous work from our group, and the lysis plasmid was constructed by taking the lysis gene, *E*, from the ePop plasmid via PCR and cloning it into a vector (Chlor, p15A) under the control of the *luxI* promoter[13,15]. The *hlyE* gene was obtained via PCR from the genomic DNA of MG1655, while mouse CCL21 and CDD-iRGD were synthesized. These genes were cloned into the lysis plasmid, under the control of either the *tac* or *luxI* promoters (Extended Data Fig. 5). Co-culturing was performed with HeLa cells and either motile or non-motile *S.* Typhimurium, SL1344 (Extended Data Table 1). For full strain and plasmid information, please refer to the Supplementary Information.

Microfluidics and microscopy. The microfluidic devices and experiment preparation protocols used in this study are similar to those previously reported from our group[13]. The bacteria growth chambers were $100 \times 100\,\mu m$ in area and approximately $1.4\,\mu m$ in height. For co-culture experiments on the chip, we first loaded a suspended culture of HeLa cells in the device media channels at very low flow rates, to allow for adherence, and then incubated the device in a tissue culture incubator for 0.5–2 days to allow for proliferation. On the day of the experiment, the device was transferred to the microscope and circuit-containing bacteria were loaded in the growth chambers before imaging. Acquisition of images was performed with a Nikon TI2 using a Photometrics CoolSnap cooled CCD camera. The scope and accessories were programmed using the Nikon Elements software.

Co-cultures for well plate experiments were performed in Falcon 96-well tissue culture plates. HeLa cells were allowed to adhere to the wells before the addition of bacteria and subsequent imaging under the microscope or measurement in a TECAN Infinite M200 Pro plate reader. For viability measurements using an MTT assay, there were two technical replicates per well. For fluorescence measurements of co-cultures with variable seeding densities of bacteria, there were three technical replicates per case.

Additional details on microfluidics and microscopy can be found in the Supplementary Information.

***In vivo* experiments.** All animal work was approved by the committee on animal care (MIT, protocol 0414-022-17). The protocol requires animals to be euthanized when tumors reach 2 cm³, or under veterinary staff recommendation. The cell line (MC26-LucF, Tanabe laboratory, Massachusetts General Hospital) was obtained from, and authenticated by, the Tanabe laboratory, MGH. The cell line was tested several times to be mycoplasma-free before implantation in mice. Sample sizes for mice were determined by expected effect size to produce a power of 0.8–0.9. Mice were blindly randomized into various groups using a random number generator.

Subcutaneous tumour model. Animal experiments were performed on 6-week-old female BALB/c mice (Taconic Biosciences) with bilateral subcutaneous hind flank tumours from an implanted mouse colon cancer cell line. The concentration for implantation of the tumour cells was 10^8 cells per ml in DMEM (no phenol red). Cells were then implanted subcutaneously at a volume of $100\,\mu l$ per flank, with each implant consisting of 10^7 cells. Tumours were typically grown to an average of $300\,mm^3$ before experiments.

Experimental liver metastasis model. The experimental metastasis model was generated by injecting luciferase-producing mouse cancer cells into surgically externalized spleens of immunocompetent mice. Tumour cells seeded the liver during 90 s, after which the spleen was removed to prevent ectopic tumour growth[30]. The MC26-LucF cell line was used (Tanabe Laboratory, MGH) and injected at 5×10^4 cells per $100\,\mu l$ PBS into the spleens of female BALB/c mice at 6 weeks of age (Taconic Biosciences.). For the liver metastasis model, tumours were grown for 5–7 days to an average total tumour burden of $143\,mm^3$ before experiments.

Bacterial growth and administration. Bacterial strains were grown overnight in LB media containing appropriate antibiotics and 0.2% glucose as for the *in vitro* experiments. A $1:100\times$ dilution in fresh media with antibiotics was started the day of injection and grown until an OD <0.1 to prevent bacteria from reaching the quorum threshold (for SLC specifically). Bacteria were spun down and washed 2 to 3 times with sterile PBS before injection into mice. Intratumoural injections of bacteria were performed at a concentration of 5×10^7 cells per ml in PBS with a total volume of 10–$20\,\mu l$ injected per tumour, while intravenous injections were given at a total volume of $100\,\mu l$. For the SLC-3 strains injection, this final volume was equally divided between the three strains at the indicated density. For liver metastasis experiments, bacteria were grown in LB media containing appropriate antibiotics and 0.2% glucose until they reached an OD of 0.05, after which they were concentrated to 10^9 to 5×10^9 bacteria per ml and delivered via oral gavage.

Post-administration monitoring for subcutaneous liver metastasis models. Luminescent signal was measured with the IVIS spectrum *in vivo* imaging system following bacterial injection. Measurements were compared relative to pre-injection values to follow dynamics. Subcutaneous tumour volume was quantified using calipers to measure the length, width, and height of each tumour throughout the imaging course ($V = L \times W \times H$). Volumes were compared to pre-injection values to follow physical tumour growth. Survival of mice was measured as the time from the beginning of the experiment up to the day when mice were moribund and euthanized. Survival for the experiment in Fig. 4f was measured with two biological replicates.
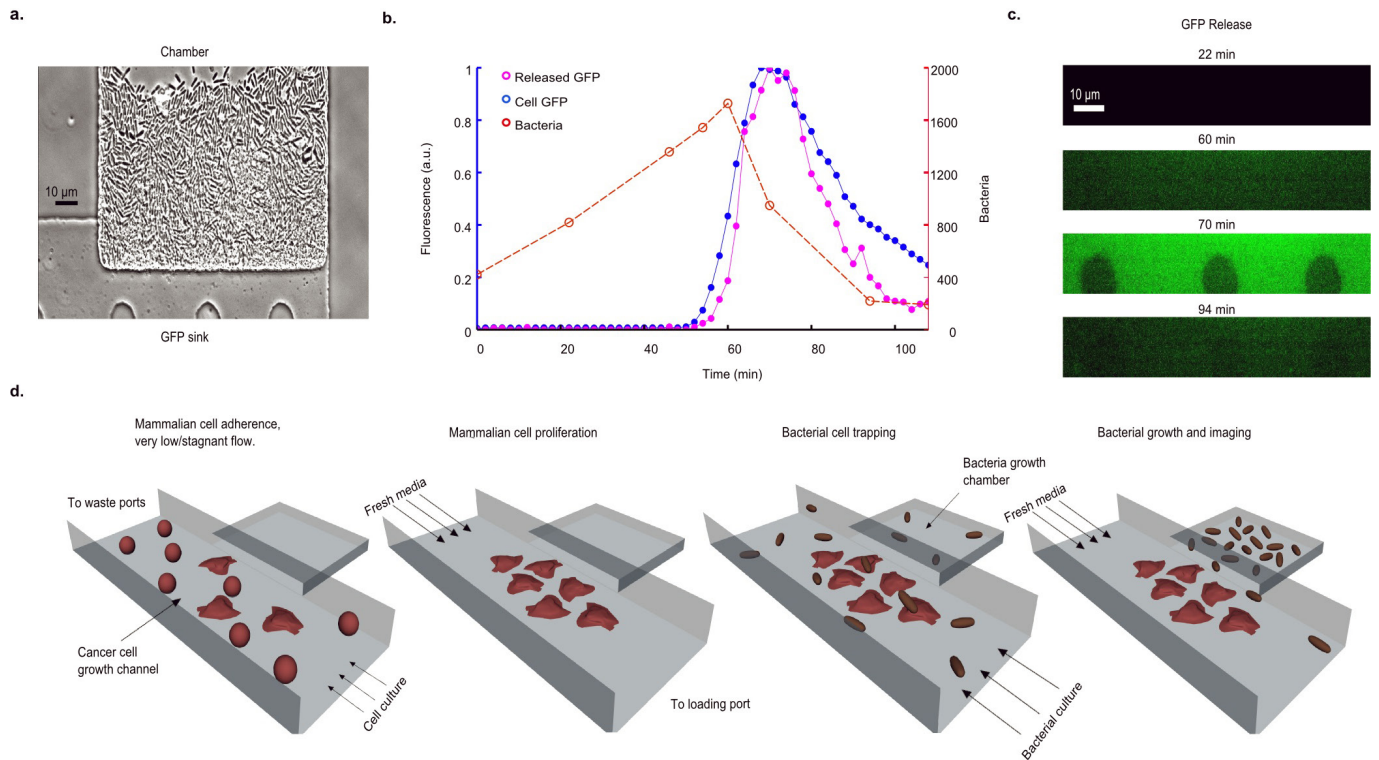
Statistical analysis. Statistical tests were calculated either in Excel (Student's *t*-test) or GraphPad Prism 5.0 (ANOVA with Bonferroni post-test, log-rank test). The details of the statistical tests carried out are indicated in the respective figure legends. Where data were approximately normally distributed, values were compared using either a Student's *t*-test or one-way ANOVA for single variable, or a two-way ANOVA for two variables. Mice were randomized in different groups before experiments.

30. Soares, K. C. *et al.* A preclinical murine model of hepatic metastases. *JoVE* e51677 (2014).

a.

b.

98 min   118 min   160 min   250 min   268 min   306 min

c.

d.
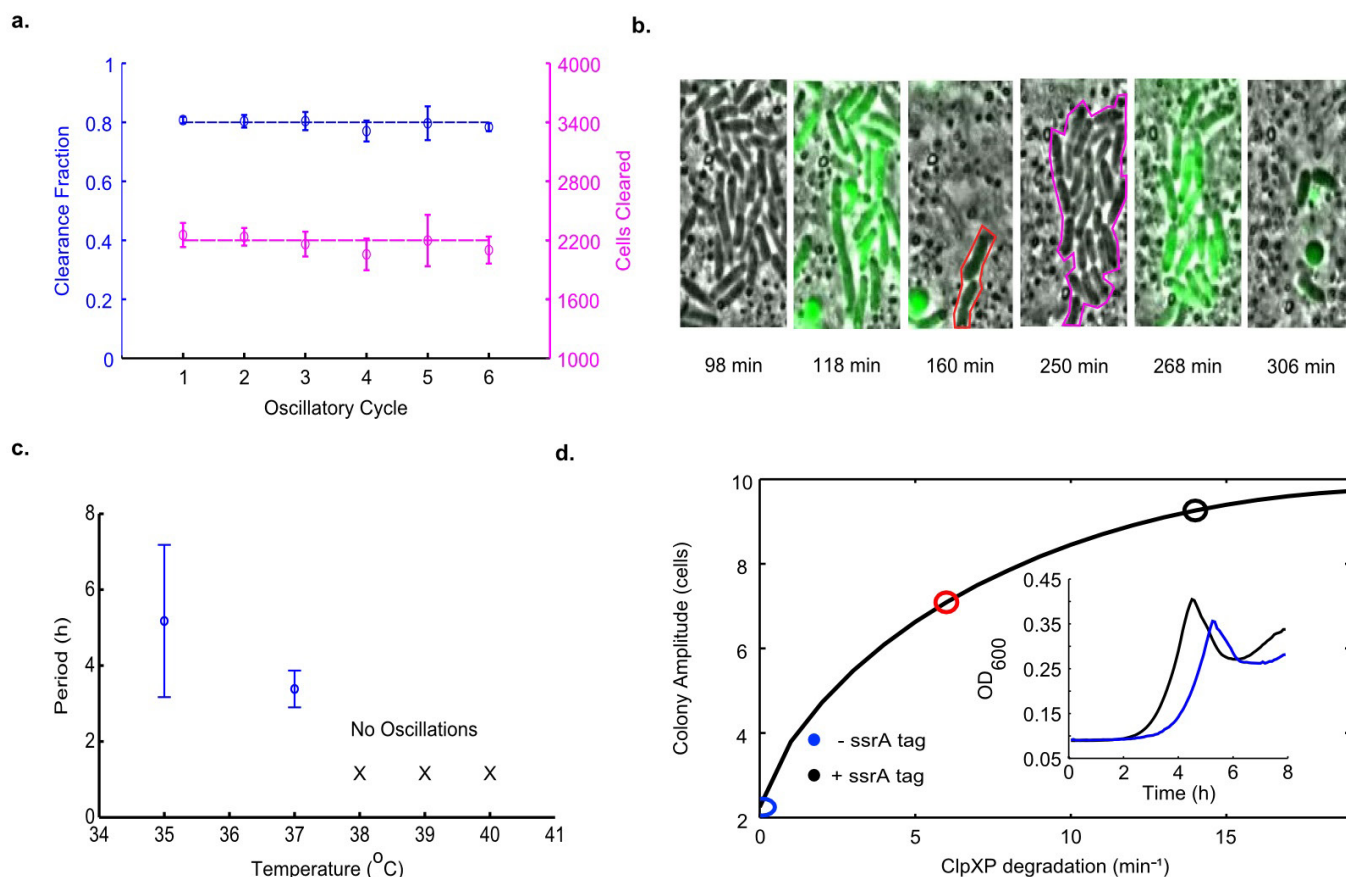
Extended Data Figure 1 | Various properties of the SLC. a, The fraction and number of bacterial cells cleared per consecutive oscillatory cycle in the growth chamber for a typical microfluidic experiment for *S. typhimurium*, including the effects of lysis and flow of cells outside of the trap (strain 1). **b**, Subset of time series images from the experiment in a showing a portion of the growth chamber where survivors of the initial lysis event (160 min frame, red outline) produce progeny (250 min frame, magenta outline) which are lysis sensitive. **c**, Period as a function of the environmental temperature for *E. coli* (strain 13). The circuit does not oscillate for temperatures above 37 °C in *E. coli*. Error bars indicate ± 1 s.d. for 12–19 peaks. **d**, Colony amplitude at quorum firing for increasing degradation on the LuxI activator protein in the computational model. These simulation results are supported by batch well-plate experiments of the LuxI ssrA (black, strain 2) and non-ssrA (blue, strain 1) tagged versions of the circuit in *S.* Typhimurium (inset).

a.

Chamber

10 μm

GFP sink

b.

c.

GFP Release

d.

Mammalian cell adherence, very low/stagnant flow.

To waste ports

Cancer cell growth channel

Cell culture

Mammalian cell proliferation

Fresh media

To loading port

Bacterial cell trapping

Bacteria growth chamber

Bacterial culture

Bacterial growth and imaging

Fresh media

Extended Data Figure 2 | Investigating lysis-mediated intracellular release. a, A bacterial growth chamber with a 0.4 μm high sink for sfGFP visualization after release. **b**, Number of bacteria (red), bacterial fluorescence (blue), sink fluorescence (pink) for a typical oscillatory cycle (strain 1). **c**, Fluorescence time series images of the microfluidic sink from **b**. **d**, General procedure for performing bacterial and cancer cell co-culture experiments in a microfluidic device (also see Supplementary Information).
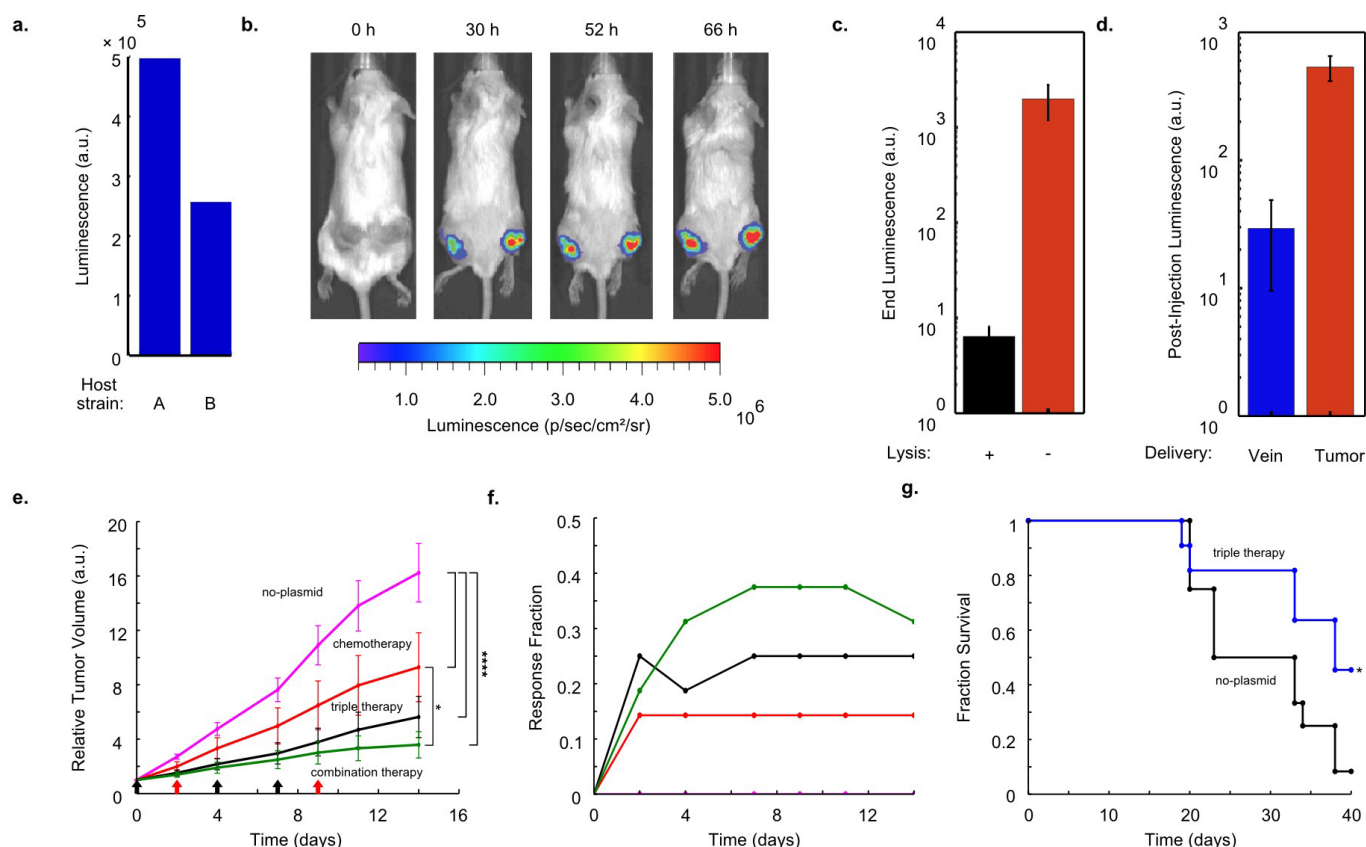
Extended Data Figure 3 | *In vivo* expression and therapy testing.
a, End-point *in vitro* luminescence intensity for SLC strains after ∼20 h of growth. Host strains A and B are the host bacteria for strains 8 and 10. They are ELH1301 and ELH 430, respectively. Host A exhibits around twofold higher luminescence with the same circuit than host B. **b**, *In vivo* imaging over time of a mouse bearing subcutaneous tumours injected with a genomically integrated constitutively luminescent strain (strain 9). **c**, End-point *in vivo* bacterial luminescence of the SLC-hly strain and the constitutively luminescent strain from the experiments presented in Fig. 4. Error bars represent the s.e.m. bacterial luminescence from 9 tumours. **d**, Post-injection *in vivo* bacterial luminescence for the constitutively luminescent strain administered intravenously (vein) or intratumorally (tumour). Luminescence was measured ∼20 h post-injection. Error bars

represent s.e.m. bacterial luminescence from 6 and 9 tumours for the intravenous and intratumoural cases, respectively. **e**, Average relative tumour volume over time for subcutaneous tumour bearing mice injected with the no-plasmid bacterium (strain 7), 5-FU chemotherapy, the SLC-3 strains, and the combination of SLC-3 with chemotherapy. Bacteria were injected intratumorally on days 0, 4, and 7 (black arrows), and chemotherapy was administered on days 2 and 9 (red arrows) (*$P < 0.05$, ****$P < 0.0001$, two-way ANOVA with Bonferroni post-test, $n = 12$–16 tumours, error bars represent s.e.). **f**, Fraction of mice from the cases in **e** which respond with 30% reduction of tumour volume over time. **g**, Fraction survival over time for mice with hepatic colorectal metastases fed with either the SLC-3 strains (blue) or the no-plasmid control (black) (*$P < 0.05$, log rank test; $n = 11$–12 mice).

a.
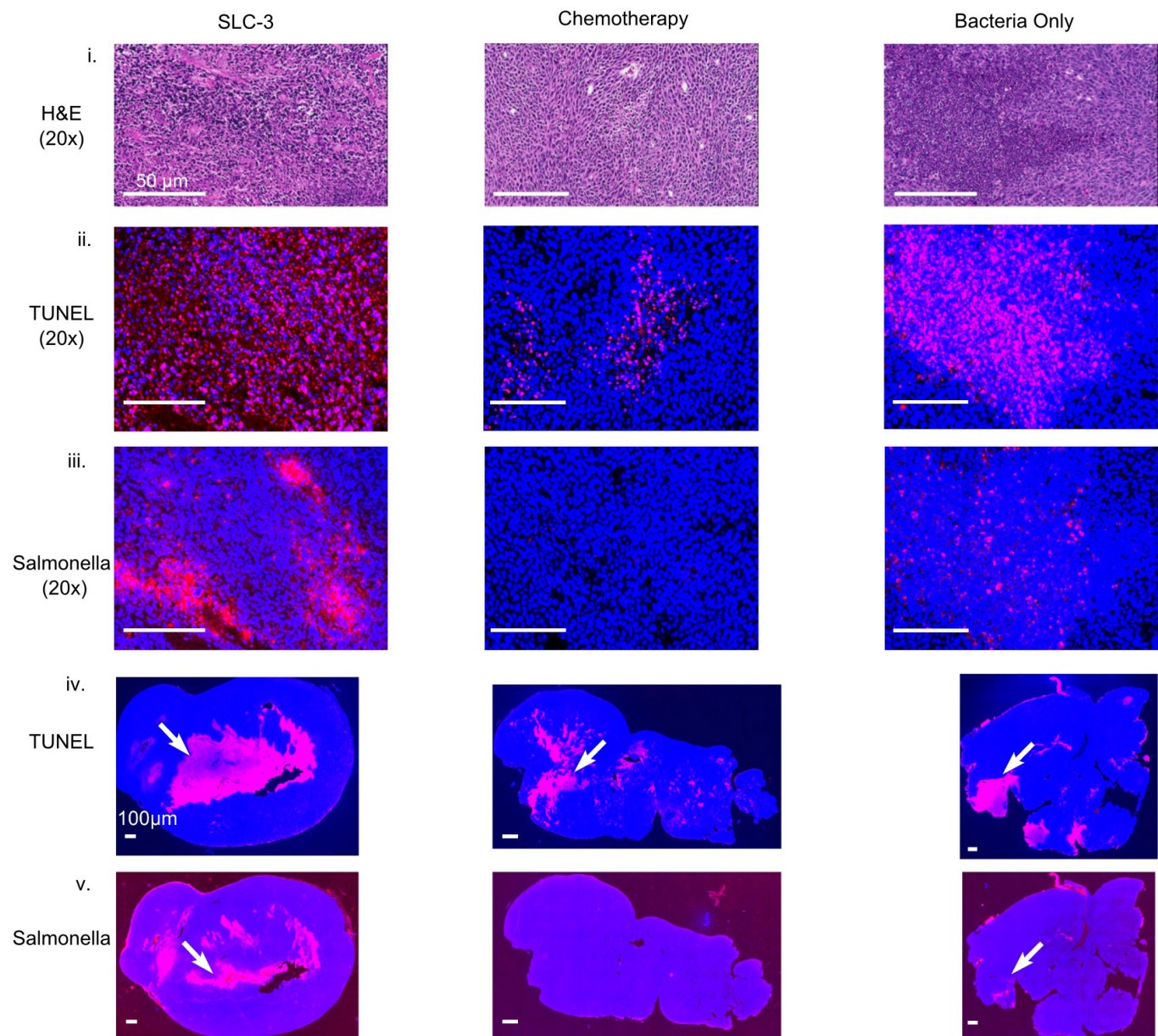
Extended Data Figure 4 | Histological analysis of tumour sections.
a, Histology of tumour sections taken from mice with different treatments 3 days post-administration. Haematoxylin and eosin staining for tissue sections intravenously injected with a combination of therapeutic bacteria (SLC-3), chemotherapy (5-FU), or a bacteria control with no therapeutic (strain 7) (i); TUNEL staining (red) in the same sections indicating cell apoptosis (ii); *Salmonella* immunohistochemistry (red) in the same sections confirming presence of bacteria in tumours (iii). Scale bars for (i–iii) denote 50 μm. TUNEL (iv) and *Salmonella* (v) staining (red) in the entire tumour sections (examples indicated by arrows). Scale bars for iv and v denote 100 μm. DAPI staining (blue) was used to obtain a measure of live and dead cells in ii–iv. Histology slices ($n = 6$) from 20× images were compared across the groups and mean intensity of TUNEL staining, normalized by sample area, was demonstrated to be significantly higher for SLC-3 compared to the other two groups ($P < 0.0001$, one-way ANOVA), and not significantly different between the chemotherapy and bacteria-only cases.

a.
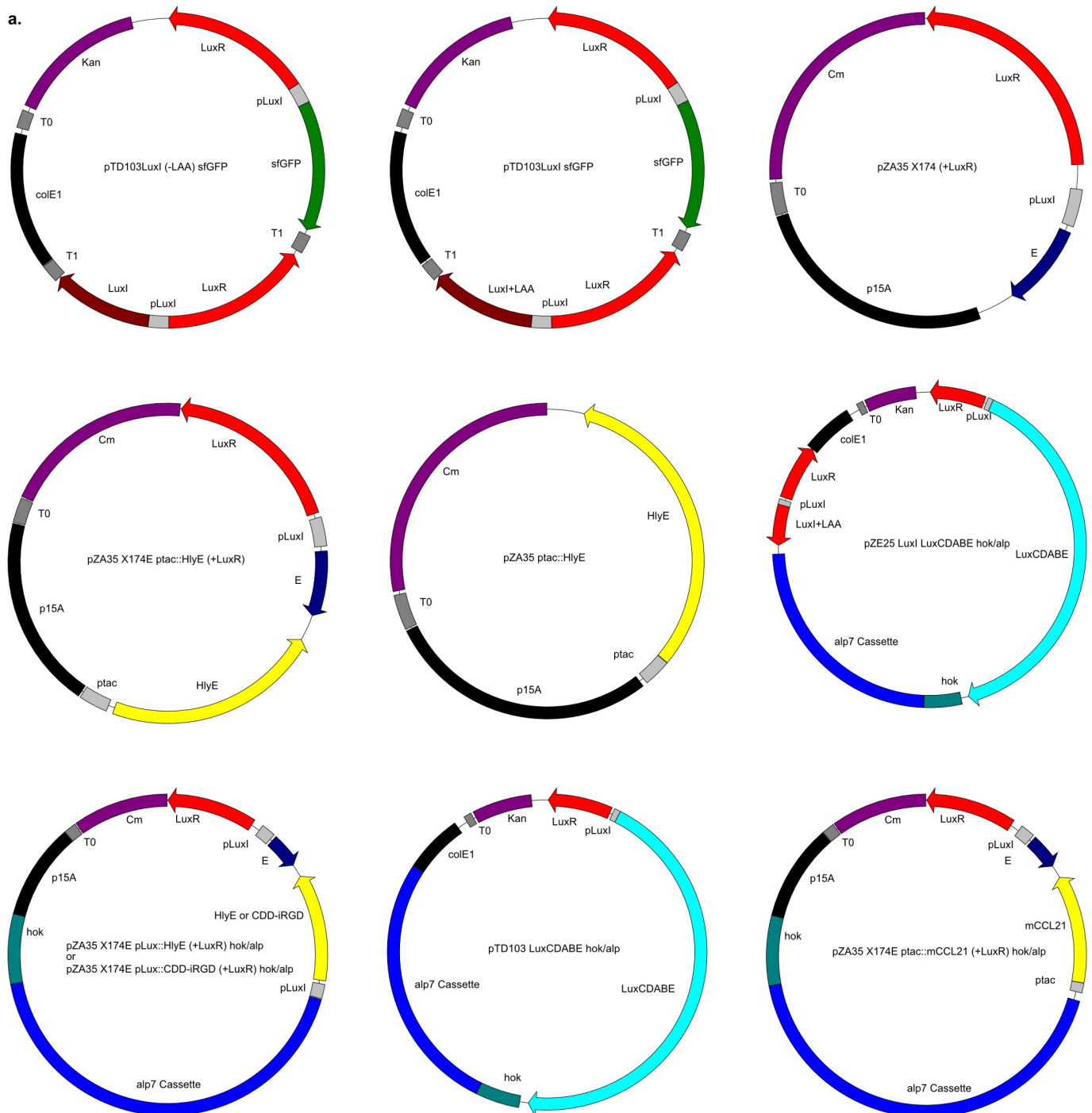
Extended Data Figure 5 | The main plasmids used in this study. See Supplementary Information for more details.

Extended Data Table 1 | A list of strains and respective plasmids used in this study

Strain #	Strain Name	Host Bacterium	Plasmid(s)
1	MOD47	SL1344, M913	pTD103 luxI (-LAA) sfGFP + pZA35 X714E (+LuxR)
2	MOD46a	SL1344, M913	pTD103 luxI sfGFP + pZA35 X714E (+LuxR)
3	MOD67	SL1344, M913	pTD103 luxI (-LAA) sfGFP + pZA35 X714E (+LuxR) ptac::HlyE
4	MOD61	SL1344, ELH1301	pTD103 luxI sfGFP + pZA35 X714E (+LuxR) ptac::HlyE
5	MOD64	SL1344, ELH1301	pTD103 luxI sfGFP + pZA35 X714E (+LuxR)
6	MOD65	SL1344, ELH1301	pZA35 ptac::HlyE
7	ELH1301	SL1344, ELH1301	N/A
8	MOD105	SL1344, ELH430	pZE25 luxI luxCDABE hok/alp + pZA35 X714E (+LuxR) pLux::HlyE hok/alp
9	EcN-luxCDABE	Nissle 1917	N/A
10	MOD101	SL1344, ELH1301	pZE25 luxI luxCDABE hok/alp + pZA35 X714E (+LuxR) pLux::HlyE hok/alp
11	MOD102	SL1344, ELH1301	pZE25 luxI luxCDABE hok/alp + pZA35 X714E (+LuxR) ptac::HlyE hok/alp
12	MOD69	SL1344, ELH1301	pTD103 LuxCDABE hok/alp + pZA35 X714E (+LuxR) ptac::HlyE hok/alp
13	MOD29	JS006, BW25113	pTD103 luxI sfGFP + pZA35 X714E (+LuxR)
14	MOD110	SL1344, ELH1301	pZE25 luxI luxCDABE hok/alp + pZA35 X714E (+LuxR) pLux::CDD-iRGD hok/alp
15	MOD112	SL1344, ELH1301	pZE25 luxI luxCDABE hok/alp + pZA35 X714E (+LuxR) ptac::mCCL21 hok/alp

See Supplementary Information for more details.